Shahid Chamran University of Ahvaz

Iranian Association of Electrical and Electronics Engineers

Journal of Applied Research in Electrical Engineering

E-ISSN: 2783-2864
P-ISSN: 2717-414X
Homepage: http://jaree.scu.ac.ir/

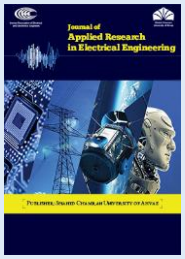

Research Article

On the Cramer-Rao Lower Bound Based Analysis of Direct Position Determination and DOA Position Finding for Co-Channel Emitter Localization

Ali Eshkevari, and Seyed Mohammad Sajad Sadough*

Faculty of Electrical Engineering, Shahid Beheshti University, Tehran 1983969411, Iran

* *Corresponding Author Email: s_sadough@sbu.ac.ir*

Abstract: Direct Position Determination (DPD) is known as an optimal, single-step technique for localizing co-channel signal sources since it processes the data gathered from all the array receiver elements together. In contrast, the commonly used radio location techniques include two independent stages. First, they estimate some initial parameters like direction, time, time-difference, frequency of arrival, etc., or their combination, and second, they localize signal sources using the triangulation of loci generated by the first stage. This disjoint structure leads to the sub-optimality of conventional localization algorithms. In this paper, we compare the Location root-mean-square-Error Lower Bounds (LELB) for DPD and position finding by DOA (PF-DOA) to prove the superiority of DPD over PF-DOA, which are commonly used for tactical fields or outdoor applications. Moreover, we demonstrate the advantages of DPD for indoor localization applications compared to PF-DOA techniques in terms of localization accuracy. We also introduce the single-group-array (SGA) structure for DPD in indoor applications and reveal that it outperforms both the PF-DOA and DPD with a classical multi-group-array (MGA) structure.

Keywords: Direct position determination, direction of arrival, co-channel signals, accuracy, Cramer-Rao lower bound.

Article history
Received 12 July 2021; Revised 09 September 2021; Accepted 25 September 2021; Published online 24 February 2022.

How to cite this article
A. Eshkevari, and S. M. S. Sadough, "On the Cramer-Rao lower bound based analysis of direct position determination and DOA position finding for co-channel emitter localization," *J. Appl. Res. Electr. Eng.*, vol. 1, no. 2, pp. 131-138, 2022.
DOI: 10.22055/jaree.2021.37946.1032

1. INTRODUCTION

1.1. Background

During the recent decades, there has been a growing interest in the localization of co-channel signal sources by using array signal processing techniques. Civil radio frequency band monitoring, wildlife protection, seismology, sonar, and defense are some of prevalent outdoor localization applications. More recently, thanks to technical improvements, some indoor localization applications have also attracted attention, especially in the medical labs where wireless medical telemetry systems (WMTS) are an instance of non-invasive medical diagnose procedures [1].

From the estimation theory viewpoint, conventional localization techniques are sub-optimal since they have two separated stages. First, they estimate some initial parameters such as the direction of arrival (DOA), time of arrival (TOA), time-difference of arrival (TDOA), or frequency-difference of arrival (FDOA), or the received signal strength (RSS), and second, they intersect the outcome loci from the first stage to localize the targets. As a matter of fact, the DOA-based position finding (PF-DOA) can be considered as the most commonly-used localization method.

Direct position determination (DPD) has lately been proposed as a single-step optimal technique for multiple co-channel signal localization by jointly using all data captured from sensor elements of all arrays. DPD is a statistical approach that uses a spatial-benefit function (SBF) whose peaks or extrema locate the signal transmitters. The SBF is the outcome of a mathematical solution to the localization problem, which is based on the statistical properties (normally covariance matrix) of the signals sensed on the array elements. These solutions are commonly referred to as *beamformers*. However, higher accuracy of the DPD method can be achieved at the expense of some extra hardware capabilities, such as synchronous sampling of all grouped receiver elements.

The main contribution of this paper consists of deriving Cramer-Rao lower bound (CRLB) based formulations of Location root-means-square-Error (LELB) for DPD and PF-

DOA methods in a unified framework. We also compare these bounds both analytically and numerically for outdoor and indoor applications to prove the superiority of DPD over traditional PF-DOA methods. Moreover, we propose a new structural deployment of the antenna hardware referred to as single-group-array (SGA) instead of the commonly used multi-group-array (MGA) to provide increased accuracy for DPD in indoor applications. Finally, we compare the DPD-SGA and DPD-MGA methods in both analytical and numerical ways in a WMTS lab scenario.

1.2. Literature Survey

Despite the long-time background of the PF-DOA methods, the extraction of CRLB for DOA estimation and PF-DOA is relatively recent. The CRLB for DOA estimation using vector and higher-order sensor arrays is presented in [1]. A conditional CRLB for DOA estimation and array calibration is provided in [2]. Moreover, a stochastic CRLB analysis for DOA estimation in the spherical harmonic's domain is addressed in [3]. More recently, a derivation and comparison of CRLB are presented in [4] for DOA estimators under the partial relaxation framework. Also, a CRLB analysis of data fusion for fingerprinting localization in non-line-of-sight (NLOS) environments is introduced in [5]. Moreover, a CRLB for DOA estimation exploiting multiple frequency pairs is provided in [6].

DPD was first proposed by Weiss et al. in 2004 for tactical field applications in their attempt to show that it exactly coincides with the maximum-likelihood (ML) estimation [7]. In [8] and [9], DPD is presented using different beamformers such as minimum-variance-distortionless-response (MVDR) and multiple-signal-classification (MUSIC), respectively. A comprehensive performance analysis of DPD with both MVDR and MUSIC beamformers is demonstrated in [10, 11]. Some DPD applications for wideband systems like radar and OFDM radios are provided in [12] and [13], respectively. In addition, a performance analysis of DPD using MUSIC algorithm is presented in [14]. Recently, a comparison of DPD performance using MVDR or MUSIC beamformers is demonstrated in [15]. A novel idea about applying free-space loss (FSL) in DPD problem formulation to have a more realistic path-length-dependent channel model is proposed more recently in [16]. Furthermore, a unified subspace fitting framework and its performance analysis for direct position determination in the presence of multipath propagation is addressed in [17]. In addition, a DPD method in asynchronous sensor networks is recently addressed in [18].

Table 1: Nomenclature used throughout the paper.

Symbol	Meaning
$\{.\}^*$	Complex conjugate
$\{.\}^T$	Transpose
$\{.\}^H$	Hermitian (conjugate transpose)
$\circ$	Hadamard product of matrices
$\otimes$	Kronecker product of matrices
tr(.)	Trace of a matrix
diag(.)	Diagonal matrix of a vector
blkdiag(.)	Block diagonal matrix of matrices
$\|.\|$	Frobenius norm of a matrix
$\boldsymbol{I}_N$	Identity matrix of size N
$\boldsymbol{J}_N$	Exchange matrix of size N
$\boldsymbol{U}_N$	All-one matrix of size N

There are some recent works on the localization of wireless capsule endoscopy (WCE) as a commonly used indoor localization application for WMTS. Pioneering research on the accuracy of RF positioning in multi-capsule endoscopy is demonstrated in [19]. A method of DOA-based endoscopy capsule localization and orientation estimation via unscented Kalman filtering is addressed in [20]. Moreover, a positioning algorithm for WCE based on RSS is provided in [21]. A review of localization strategies for robotic endoscopic capsules is presented in [22].

1.3. Nomenclature

The conventions and notations presented in Table 1 will be used throughout the paper. Moreover, the DOA or azimuth angles are considered in navigation (clock oriented) and not in trigonometric mode.

2. Problem Formulation

Consider M properly separated L-element receiving sensor arrays with similar *shapes* and *orientations*. We assume K sources transmitting unknown uncorrelated narrowband (NB) signals with baseband or *analytical* equivalents $s_k(t), k = 1, \dots, K$, located at enough distance from the receiving arrays satisfying far-field conditions. All transmitters and receiver sensors are assumed to be stationary during the observation period, so there is no Doppler frequency shift in the model. We aim at localizing transmitters using the sensors observed signals. The position of the k-th transmitter is denoted by the two- or three-dimensional (2D or 3D) vector $\boldsymbol{p}_k$. The NB analytical signal observed at the m-th array is given by an $L \times 1$ vector during the time interval $0 \le t \le T$ as

$$\boldsymbol{x}_m(t) = \sum_{k=1}^{K} \boldsymbol{a}_m(\boldsymbol{p}_k) H_m(\boldsymbol{p}_k) \boldsymbol{s}_k(t) + \boldsymbol{b}_m(t), \quad (1)$$

where $\boldsymbol{a}_m(\boldsymbol{p}_k)$ is the m-th array response to a signal emitted from $\boldsymbol{p}_k$, $H_m(\boldsymbol{p}_k)$ is a complex scalar characterizing the channel response between $\boldsymbol{p}_k$ and the (reference point of) m-th array, and $\boldsymbol{b}_m(t)$ denotes the zero-mean, circular complex AWGN with variance σ^2 at the m-th array receiver. The transmitters are assumed constant during a localization period, i.e., we assume M quasi-static channels. The observation time interval is $T \gg \max(\tau_m(\boldsymbol{p}_k))$ for the region of interest where $\tau_m(\boldsymbol{p}_k)$ is the propagation delay between $\boldsymbol{p}_k$ and the reference point of the m-th array. Assuming enough distance between transmitters and receiver arrays, which makes the array responses only dependent on the DOA of the received signals, (1) can be expressed as

$$\boldsymbol{x}_m(t) = \sum_{k=1}^{K} \boldsymbol{a}_m(\phi_{mk}) H_{mk} \boldsymbol{s}_k(t) + \boldsymbol{b}_m(t), \quad (2)$$

where ϕ_{mk} is the north-oriented polar coordinate representation of the DOA of the signal received at the m-the array from $\boldsymbol{p}_k$, and:

$$H_{mk} = H(d_{mk}, \alpha_{mk}) = \alpha_{mk}\, g_{mk} \frac{d_0}{d_{mk}} \mathrm{e}^{-j2\pi \frac{d_{mk}}{\lambda}} \quad (3)$$

is the *channel response* between the m-th array and k-th transmitter with path length d_{mk}, for a carrier with wavelength λ, where α_{mk} characterizes all the stochastic

gains and attenuations through the channel path including the fading effect, d_0 is the normalizing distance to consider FSL in channel response (e.g., 10λ), and g_{mk} is the deterministic channel gain at distance d_0 from the k-th transmitter. The FSL is taken into account to produce a so-called dynamic sensor-array response (DSAR) according to [16]. The sample matrix version of (2) for N snapshots of signals is in the following form

$$\boldsymbol{X}_m = \boldsymbol{A}(\boldsymbol{\phi}_m)\boldsymbol{H}_m\boldsymbol{S} + \boldsymbol{B}_m\,, \tag{4}$$

Where:

$$\boldsymbol{\phi}_m \triangleq [\phi_{m1}, \dots, \phi_{mK}]^T, \tag{5}$$

and

$$\boldsymbol{H}_m \triangleq \mathrm{diag}([H_{m1}, \dots, H_{mK}]). \tag{6}$$

To calculate the CRLB of our estimation problem, we need the sample covariance matrix of sensed signals $\boldsymbol{X}_m$ [23], which is defined as

$$\boldsymbol{R}_m \triangleq \frac{1}{N}\boldsymbol{X}_m\boldsymbol{X}_m^H\,, \tag{7}$$

2.1. PF-DOA Formulation

In a PF-DOA problem of co-channel signals, the DOAs of impinging waves to each array are estimated independently and without considering other arrays. The signal received at the reference point of the m-th array can be expressed as

$$s_{mk}(t) \triangleq H_{mk}\, s_k(t), \tag{8}$$

so, Eq. (4) can be written as

$$\boldsymbol{X}_m = \boldsymbol{A}(\boldsymbol{\phi}_m)\boldsymbol{S}_m + \boldsymbol{B}_m, \tag{9}$$

where $\boldsymbol{X}_m$ and $\boldsymbol{B}_m$ are $L \times N$ matrices of the sample received signals and noise for sensor elements of the m-th array, respectively, and $\boldsymbol{S}_m$ is the $K \times N$ sample matrix of the signals received at the reference point of the m-th array. The sample covariance matrix of (7) is in the form of

$$\boldsymbol{R}_m \triangleq \boldsymbol{A}(\boldsymbol{\phi}_m)\boldsymbol{R}_{Sm}\boldsymbol{A}^H(\boldsymbol{\phi}_m) + \boldsymbol{R}_{Bm}\,, \tag{10}$$

where source signals and noise sample covariance matrices are defined as

$$\boldsymbol{R}_{Sm} \triangleq \tfrac{1}{N}\boldsymbol{S}_m\boldsymbol{S}_m^H\,,\ \boldsymbol{R}_{Bm} \triangleq \tfrac{1}{N}\boldsymbol{B}_m\boldsymbol{B}_m^H\,. \tag{11}$$

2.2. DPD Formulation

In a DPD problem of co-channel signals, the locations of signal emitters are estimated using signals sensed in all arrays together. Here, we define the pointing vector of the m-th array's reference point to position $\boldsymbol{p}_k$ as

$$\tilde{\boldsymbol{a}}_m(\boldsymbol{p}_k) \triangleq \boldsymbol{a}(\phi_{mk})H_{mk}\,, \tag{12}$$

so, Eq. (4) can be written as

$$\boldsymbol{X}_m = \tilde{\boldsymbol{A}}_m(\boldsymbol{P})\boldsymbol{S} + \boldsymbol{B}_m\,, \tag{13}$$

where $\boldsymbol{X}_m$ and $\boldsymbol{B}_m$ are $L \times N$ matrices of the sample received signals and noise for sensor elements of the m-th array, respectively, and $\boldsymbol{S}$ is the $K \times N$ sample matrix of the emitted signals. The sample covariance matrix of (7) is in the form of

$$\boldsymbol{R}_m \triangleq \tilde{\boldsymbol{A}}_m(\boldsymbol{P})\boldsymbol{R}_S\tilde{\boldsymbol{A}}_{\boldsymbol{m}}^H(\boldsymbol{P}) + \boldsymbol{R}_{Bm}\,, \tag{14}$$

where source signals and noise sample covariance matrices are defined as

$$\boldsymbol{R}_S \triangleq \frac{1}{N}\boldsymbol{S}\boldsymbol{S}^H\,,\qquad \boldsymbol{R}_{Bm} \triangleq \frac{1}{N}\boldsymbol{B}_m\boldsymbol{B}_m^H\,. \tag{15}$$

Finally, the global covariance matrix of all sensors will be

$$\boldsymbol{R} \triangleq \mathrm{blkdiag}(\boldsymbol{R}_1. \dots . \boldsymbol{R}_M)\,. \tag{16}$$

The dimensions of $\boldsymbol{R}$ in (16) are $U \times U$ where $U = LM$.

3. Derivation of the Cramer-Rao Lower Bound

In array processing theory, whenever a single snapshot is assumed to be a zero-mean Gaussian random variable, and when successive snapshots are supposed to be statistically independent, the (i,j)-th element of the Fisher information matrix (FIM) for any parameter estimation is defined as [23]

$$\boldsymbol{F}_{ij} = -N\,\mathrm{tr}\left(\frac{\partial\Re^{-1}}{\partial\psi_i}\frac{\partial\Re}{\partial\psi_j}\right) = N\,\mathrm{tr}\left(\Re^{-1}\frac{\partial\Re}{\partial\psi_i}\Re^{-1}\frac{\partial\Re}{\partial\psi_j}\right), \tag{17}$$

where $\Re$ is the covariance matrix for a single snapshot, N is the number of observations of array signals, and $\boldsymbol{\psi} = [\psi_i, \psi_j]$ is the vector of the estimated parameters. The CRLB states about the unbiased estimate $\widehat{\boldsymbol{\psi}}$ that

$$\mathbf{var}(\widehat{\boldsymbol{\psi}}) \geq \mathrm{tr}(\boldsymbol{F}^{-1})\,. \tag{18}$$

There are some important considerations [23].

- The physical dimension of $\Re$ is *power*.
- $\Re$ contains information about signal and noise powers.
- $\frac{\partial\Re}{\partial\psi_i}$ contains information about the array geometry.

3.1. LELB for PF-DOA

In a PF-DOA problem, the location of any arbitrary point $\boldsymbol{p}$ in the monitoring area is determined by the estimation of DOAs of signals impinging each of the M array elements from that point. Then, for the m-th array, the estimation parameter is $\widehat{\boldsymbol{\psi}} = [\phi_m]$, and from (17), the single-element FIM (scalar) is written as

$$F_m = N\,\mathrm{tr}\left(\left[\boldsymbol{R}_m^{-1}\frac{\partial\boldsymbol{R}_m}{\partial\psi_i}\right]^2\right). \tag{19}$$

For simplicity, we rewrite (10) for the m-th array as

$$\boldsymbol{R}_m \triangleq \boldsymbol{A}\boldsymbol{R}_{Sm}\boldsymbol{A}^H + \sigma^2\boldsymbol{I}_L\,, \tag{20}$$

where σ^2 is the noise power that is supposed to be constant for all receiver elements of the whole array.

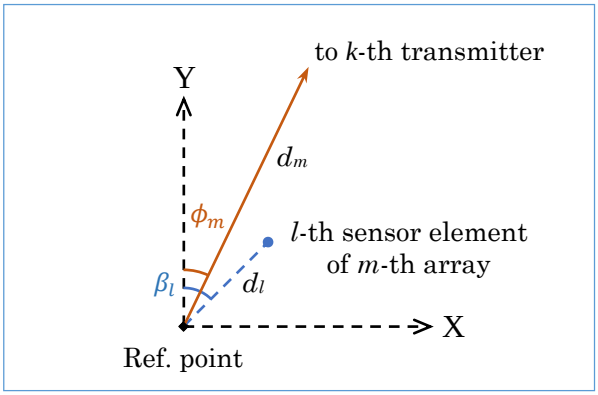

Fig. 1: Parameters definitions for $\boldsymbol{m}$-th array properties

To achieve the matrix inversion $\boldsymbol{R}_m^{-1}$, we can use direct computations, or we can apply the matrix inversion lemma to (20) as

$$\boldsymbol{R}_m^{-1} = \sigma^{-2}(\boldsymbol{I} - \boldsymbol{A}(\boldsymbol{A}\boldsymbol{A}^H + \sigma^2\boldsymbol{R}_{Sm}^{-1})\boldsymbol{A}^H)\,, \tag{21}$$

which is a proper way for a $K \times K$ diagonal matrix $\boldsymbol{R}_{Sm}$ (uncorrelated source signals at the m-th array reference point) that can be simply inverted compared with direct inversion of $L \times L$ non-diagonal $\boldsymbol{R}_m$ with $K < L$ and usually $K = 1$ for numerical analysis.

According to (20), we have

$$\frac{\partial \boldsymbol{R_m}}{\partial \phi_m} = \frac{\partial \boldsymbol{A}}{\partial \phi_m}\boldsymbol{R}_{Sm}\boldsymbol{A}^H + \boldsymbol{A}\boldsymbol{R}_{Sm}\frac{\partial \boldsymbol{A}^H}{\partial \phi_m}. \tag{22}$$

To compute the CRLB for DOA estimation of the signal emitted from the k-th transmitter, i.e., $\boldsymbol{p} = \boldsymbol{p}_k$, we notice that except for the emitter located at the point $\boldsymbol{p}_k$, other emitters are assumed to have fixed locations, so they can be ignored during the derivation procedure. We thus have

$$\frac{\partial \boldsymbol{A}}{\partial \phi_m} = \frac{\partial}{\partial \phi_m}[\boldsymbol{a}_1, \dots, \boldsymbol{a}_K] = \left[\boldsymbol{0}, \dots, \frac{\partial \boldsymbol{a}_k}{\partial \phi_m}, \dots \boldsymbol{0}\right]. \tag{23}$$

For notation simplicity, we remove the subscript k and use $\boldsymbol{a} = \boldsymbol{a}_k$. Assuming that the signal emitted from $\boldsymbol{p}$ is uncorrelated with other signals, we have

$$\frac{\partial \boldsymbol{R_m}}{\partial \phi_m} = \frac{\partial \boldsymbol{a}}{\partial \phi_m}P_m\boldsymbol{a}^H + \boldsymbol{a}P_m\frac{\partial \boldsymbol{a}^H}{\partial \phi_m} = P_m\frac{\partial(\boldsymbol{a}\boldsymbol{a}^H)}{\partial \phi_m}, \tag{24}$$

where P_m is the k-th diagonal element of $\boldsymbol{R}_{Sm}$ representing the power received at the reference point of the m-th array from the emitter at the point $\boldsymbol{p}$. According to Fig. 1, for the l-th element of $\boldsymbol{a}$, we have

$$a_l = \exp\left(j\frac{2\pi}{\lambda}d_l\cos(\beta_l - \phi_m)\right), \tag{25}$$

$$\frac{\partial a_l}{\partial \phi_m} = j\frac{2\pi}{\lambda}d_l\sin(\beta_l - \phi_m)\,a_l\,, \tag{26}$$

where d_l and β_l are the distance and angle of the l-th element with respect to the reference point of the m-th array, respectively. Then, we have

$$\frac{\partial \boldsymbol{a}}{\partial \phi_m} = j\frac{2\pi}{\lambda}\mathrm{diag}\big(\boldsymbol{\rho}(\phi_m)\big)\,\boldsymbol{a}\,, \tag{27}$$

$$\frac{\partial \boldsymbol{a}^H}{\partial \phi_m} = -j\frac{2\pi}{\lambda}\boldsymbol{a}^H\,\mathrm{diag}\big(\boldsymbol{\rho}(\phi_m)\big)\,, \tag{28}$$

where

$$\boldsymbol{\rho}(\phi_m) \triangleq j\frac{2\pi}{\lambda}\boldsymbol{d} \circ \sin(\boldsymbol{\beta} - \phi_m)\,, \tag{29}$$

where $\boldsymbol{d} = [d_1, \dots, d_L]^T$ and $\boldsymbol{\beta} = [\beta_1, \dots, \beta_L]^T$. Considering (24), we have

$$\frac{\partial \boldsymbol{R_m}}{\partial \phi_m} = P_m\boldsymbol{C}_\phi \circ (\boldsymbol{a}\boldsymbol{a}^H), \tag{30}$$

where:

$$\boldsymbol{C}_\phi \triangleq \mathrm{diag}\big(\boldsymbol{\rho}(\phi_m)\big)\,\boldsymbol{U}_L - \boldsymbol{U}_L\,\mathrm{diag}\big(\boldsymbol{\rho}(\phi_m)\big)\,. \tag{31}$$

Now, we can determine F_m, and according to CRLB about unbiased DOA estimation of $\hat{\phi}_m$, we have

$$\mathrm{var}\big(\hat{\phi}_m\big) \geq \tfrac{1}{F_m}. \tag{32}$$

Finally, due to the Euclidian summability of variances, we can write the total localization variance for a PF-DOA method (like triangulation) as

$$\mathrm{var}(\hat{\boldsymbol{p}}) \geq \frac{1}{M}\sum_{m=1}^{M} d_m^2\,\mathrm{var}\big(\hat{\phi}_m\big) = \mathrm{LELB}_{PF-DOA}\,, \tag{33}$$

where d_m is the distance between the m-th array and the signal emitter at $\boldsymbol{p}$.

Moreover, considering (20), the linear signal-to-noise-ratio (SNR) at the m-th array can be expressed as

$$\mathrm{SNR}_m = \frac{\mathrm{tr}(\boldsymbol{A}\boldsymbol{R}_{Sm}\boldsymbol{A}^H)}{L\sigma^2}, \tag{34}$$

where, according to (11), $\boldsymbol{R}_{Sm}$ is the covariance matrix of the signals received at the reference point of the m-th array (not at the transmitter's location).

3.2. CRLB and LELB for DPD

In a DPD problem, the location of any arbitrary point $\boldsymbol{p}$ in the monitoring area is directly estimated by jointly using signal observations from M numbers of the L-sensor arrays. For notational simplicity, we rewrite (14) as

$$\boldsymbol{R}_m \triangleq \widetilde{\boldsymbol{A}}_m\boldsymbol{R}_S\widetilde{\boldsymbol{A}}_{\boldsymbol{m}}^H + \sigma^2\boldsymbol{I}_L\,, \tag{35}$$

and by considering the definition of $\boldsymbol{R}$ in (16), we can write

$$\boldsymbol{R} \triangleq \widetilde{\boldsymbol{A}}\boldsymbol{R}_S\widetilde{\boldsymbol{A}}^H + \sigma^2\boldsymbol{I}_U. \tag{36}$$

So, using (17) for estimation of $\boldsymbol{\psi} = [x, y]^T$ leads to

$$\boldsymbol{F}_{ij} = N\,\mathrm{tr}\left(\boldsymbol{R}^{-1}\frac{\partial \boldsymbol{R}}{\partial \psi_i}\boldsymbol{R}^{-1}\frac{\partial \boldsymbol{R}}{\partial \psi_j}\right). \tag{37}$$

To compute $\boldsymbol{R}^{-1}$ for an MGA structure, we consider (16) as

$$\boldsymbol{R}^{-1} \triangleq \mathrm{blockdiag}\big(\boldsymbol{R}_1^{-1}, \dots, \boldsymbol{R}_M^{-1}\big)\,, \tag{38}$$

which states that we can divide the inversion problem to $\boldsymbol{M}$ inversions of smaller dimension matrices to reduce the computational load. Moreover, we can use the matrix inversion similar to (21) for calculating $\boldsymbol{R}^{-1}$ or $\boldsymbol{R}_m^{-1}$.

To calculate $\frac{\partial \boldsymbol{R}}{\partial \psi_i}$, we can use similar steps to (22)-(24) by which we get

$$\frac{\partial \boldsymbol{R}}{\partial \psi_i} = \frac{\partial \tilde{\boldsymbol{a}}}{\partial \psi_i}P\tilde{\boldsymbol{a}}^H + \tilde{\boldsymbol{a}}P\frac{\partial \tilde{\boldsymbol{a}}^H}{\partial \psi_i} = P\frac{\partial(\tilde{\boldsymbol{a}}\tilde{\boldsymbol{a}}^H)}{\partial \psi_i}, \tag{39}$$

where $\tilde{\boldsymbol{a}}$ is the k-th column of $\widetilde{\boldsymbol{A}}$ with size $U \times 1$ and P is the k-th diagonal element of $\boldsymbol{R}_S$ representing the emitting power of the source at $\boldsymbol{p}$. We have removed subscript k for notation simplicity. Considering (3), regarding the u-th element of $\tilde{\boldsymbol{a}}$, we have

$$\tilde{a}_u = \alpha_u g_u\frac{d_0}{d_u}\exp\left(-j\frac{2\pi}{\lambda}d_u\right), \tag{40}$$

$$\frac{\partial \tilde{a}_u}{\partial \psi_i} = -\left(\frac{1}{d_u} + j\frac{2\pi}{\lambda}\right)\tilde{a}_u\frac{\partial d_u}{\partial \psi_i}, \tag{41}$$

where d_u is the distance between $\boldsymbol{p}$ and the u-th sensor element. Moreover, we have

$$d_u{}^2 = (x - x_u)^2 + (y - y_u)^2\,, \tag{42}$$

$$\frac{\partial d_u}{\partial x} = \frac{x - x_u}{d_u} = \sin\phi_u \,, \tag{43}$$

$$\frac{\partial d_u}{\partial y} = \frac{y - y_u}{d_u} = \cos\phi_u \,, \tag{44}$$

where ϕ_u is the direction (azimuth) of $\boldsymbol{p}$ from u-th element's viewpoint. Therefore, for $\psi_i = x$, we have

$$\frac{\partial \tilde{\boldsymbol{a}}}{\partial x} = \text{diag}(\boldsymbol{\zeta} \circ \sin\boldsymbol{\phi})\, \tilde{\boldsymbol{a}} \,, \tag{45}$$

$$\frac{\partial \tilde{\boldsymbol{a}}^H}{\partial x} = \tilde{\boldsymbol{a}}^H \,\text{diag}(\boldsymbol{\zeta}^* \circ \sin\boldsymbol{\phi}) \,, \tag{46}$$

where $\boldsymbol{\zeta} = [\zeta_1, \dots, \zeta_U]^T$, $\zeta_u = -\left(\frac{1}{d_u} + j\frac{2\pi}{\lambda}\right)$, and $\boldsymbol{\phi} = [\phi_1, \dots, \phi_U]^T$. Using (39) and following similar steps for x and y, we have

$$\frac{\partial \boldsymbol{R}}{\partial x} = P\, \boldsymbol{C}_x \circ (\tilde{\boldsymbol{a}}\tilde{\boldsymbol{a}}^H), \tag{47}$$

$$\frac{\partial \boldsymbol{R}}{\partial y} = P\, \boldsymbol{C}_y \circ (\tilde{\boldsymbol{a}}\tilde{\boldsymbol{a}}^H), \tag{48}$$

where

$$\boldsymbol{C}_x \triangleq \text{diag}(\boldsymbol{\zeta} \circ \sin\boldsymbol{\phi})\, \boldsymbol{W} + \boldsymbol{W}\, \text{diag}(\boldsymbol{\zeta}^* \circ \sin\boldsymbol{\phi}) \,, \tag{49}$$

$$\boldsymbol{C}_y \triangleq \text{diag}(\boldsymbol{\zeta} \circ \cos\boldsymbol{\phi})\, \boldsymbol{W} + \boldsymbol{W}\, \text{diag}(\boldsymbol{\zeta}^* \circ \cos\boldsymbol{\phi}) \,, \tag{50}$$

where $\boldsymbol{W} = \boldsymbol{I}_M \otimes \boldsymbol{U}_L$.

In fact, $\boldsymbol{W}$ masks any statistical dependency between signals received by different arrays in accordance with the definition of classical DPD. Finally, we can determine the elements of $\boldsymbol{F}$ and then derive the CRLB. For an unbiased estimation $\hat{\boldsymbol{p}}$, the CRLB states that

$$\text{var}(\hat{\boldsymbol{p}}) \geq \text{tr}(\boldsymbol{F}^{-1}). \tag{51}$$

The total SNR in (36) is given by

$$\text{SNR} = \frac{\text{tr}(\tilde{\boldsymbol{A}}\boldsymbol{R}_S\tilde{\boldsymbol{A}}^H)}{U\sigma^2} \,, \tag{52}$$

and the specific SNR due to the k-th transmitter will be

$$\text{SNR}_k = \frac{\text{tr}(\tilde{\boldsymbol{a}}_k P_k \tilde{\boldsymbol{a}}_k^H)}{\sigma^2} = \frac{P_k \tilde{\boldsymbol{a}}_k^H \tilde{\boldsymbol{a}}_k}{\sigma^2}, \tag{53}$$

where P_k is the power transmitted from the k-th emitter.

Since the fading coefficients in $\tilde{\boldsymbol{a}}$ are considered constant during each observation interval of DPD estimation, we can average the CRLBs resulting from several observation intervals to achieve a more reliable criterion for the lower bound [24]. For an MGA structure we use LELB instead of CRLB abbreviation.

4. DPD For Indoor Applications

In addition to outdoor applications such as localization in tactical fields, there are some indoor applications that should be considered. An instance of common indoor localization applications is the medical lab of WMTS, which uses a frequency of about 1430 MHz in accordance with the Federal Communications Commission (FCC) rules [25].

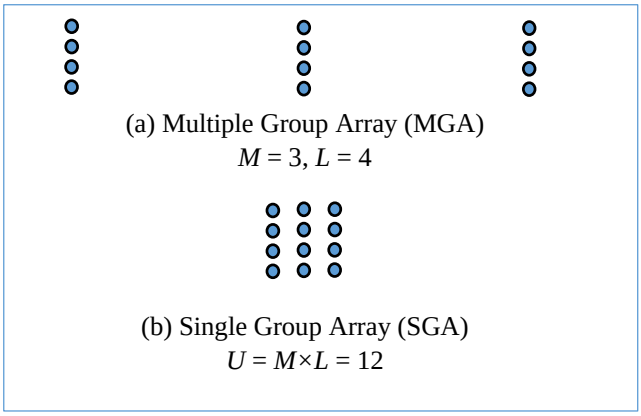

Fig. 2: Some examples of MGA and SGA structures

One essential rule in antenna array geometry is that the element spacing and the whole array dimensions should be about the carrier wavelength. This provides an opportunity for indoor applications to exploit the default localization array structure, i.e., MGA to be used as an SGA one. Fig. 2 shows the concept of MGA and SGA structures in which U is the total number of sensor elements. In DPD, the SGA structure provides more accuracy and resolution than the MGA since it takes into account the statistical dependency (covariance) between observations of all the sensor elements together, in contrast to the MGA structure that ignores any statistical dependency between the elements that belong to different groups (arrays).

For an SGA structure, (13) can be written as

$$\boldsymbol{X} = \tilde{\boldsymbol{A}}(\boldsymbol{P})\boldsymbol{S} + \boldsymbol{B} \,, \tag{54}$$

where $\boldsymbol{X}$ and $\boldsymbol{B}$ are $U \times N$ matrices of the sample received signals and noise for sensor elements of the whole array, respectively, and $\boldsymbol{S}$ is the $K \times N$ sample matrix of the emitted signals. The sample covariance matrix of (54) is in the form of

$$\boldsymbol{R} \triangleq \tilde{\boldsymbol{A}}(\boldsymbol{P})\boldsymbol{R}_S\tilde{\boldsymbol{A}}^{\boldsymbol{H}}(\boldsymbol{P}) + \boldsymbol{R}_B \,, \tag{55}$$

which is not a sparse matrix such as the global covariance matrix in (16) since the covariance between the observations of all U sensor elements of the SGA is taken into account. The rest of the CRLB extraction for the SGA structure is similar to the formulations presented in Subsection 3.2.

5. Simulations and Numerical Analysis

This section compares the numerically determined root mean square error (RMSE) of localization and analytically derived CRLB and LELB versus SNR. Each RMSE value is obtained by 100 Monte-Carlo experiments, each including 64 samples of array observations. All values are normalized to carrier wavelength.

We first consider a tactical field map, as depicted in Fig. 3. We assume three receiving arrays (M=3) where each array is composed of seven sensor elements (L=7). All arrays are similarly deployed in the uniform circular array (UCA) or uniform linear array (ULA) structures that we refer to as UCA7 and ULA7, respectively. The element spacing is equal to about half of the wavelength of a 300 MHz carrier (0.5×1 m). We assume that the transmitter is emitting an unknown signal located at point (1500, 1500) m.

Fig. 4 and Fig. 5 show the LELB normalized to wavelength versus SNR for both PF-DOA and DPD for the case of UCA and ULA array geometries, respectively. We can observe a superior performance in terms of localization accuracy achieved by DPD over PF-DOA, especially at low SNRs, for about 2-2.5 dB and 3-4 dB for UCA and ULA geometries, respectively. We have also shown the RMSE value associated with DPD using numerical analysis.

The second performance analysis is related to a typical indoor localization problem as depicted in Fig. 6 in which both MGA and SGA structures are deployed. We assume eight receiving arrays (M=8) where each array is composed of five sensor elements (L=5). All arrays are similarly deployed in the ULA structure that we refer to as ULA5. The element spacing is equal to about three times the wavelength, which is 1430 MHz carrier (3×21 cm). We assume that one transmitter is emitting an unknown signal located at point (0, 0) m at the array center.

Fig. 7 shows the LELB normalized to wavelength versus SNR for PF-DOA and DPD with MGA structure, and CRLB for DPD with SGA structure. It can be easily seen that DPD-MGA outperforms PF-DOA by about 5 dB, and DPD-SGA outperforms DPD-MGA by about 12 dB. The normalized RMSE values of DPD-MGA and DPD-SGA are presented as well using numerical analysis.

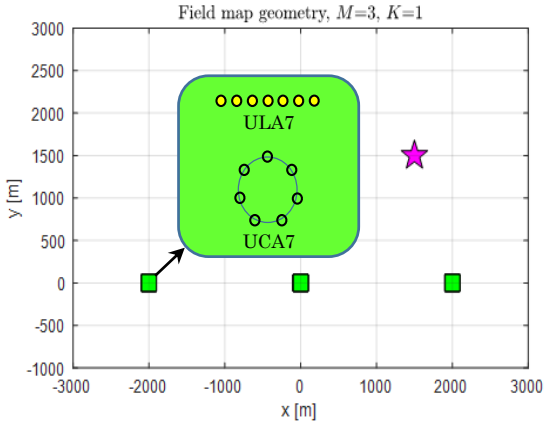

Fig. 3: The tactical field geometry considered with three 7-element ULA or UCA arrays and one transmitter.

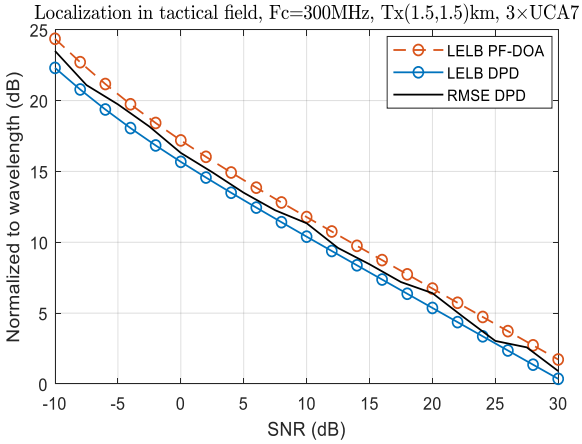

Fig. 4: The performance comparison for DPD and PF-DOA using UCA7 arrays in a typical tactical field

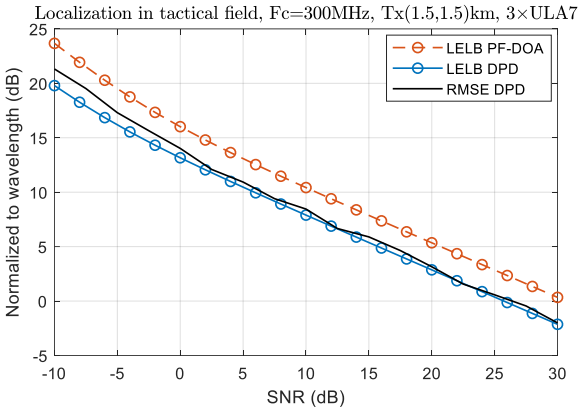

Fig. 5: The performance comparison of DPD and PF-DOA using ULA7 arrays in a typical tactical field

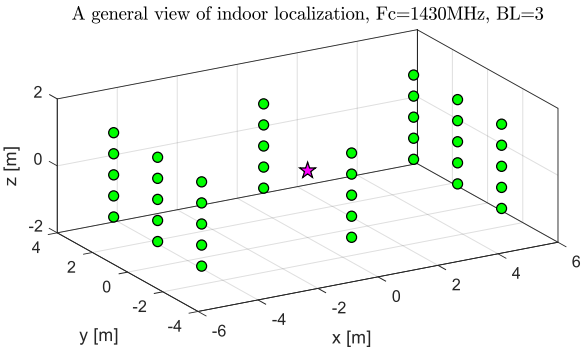

Fig. 6: A typical indoor localization application with eight 5-element ULAs as an SGA with 40 sensor elements

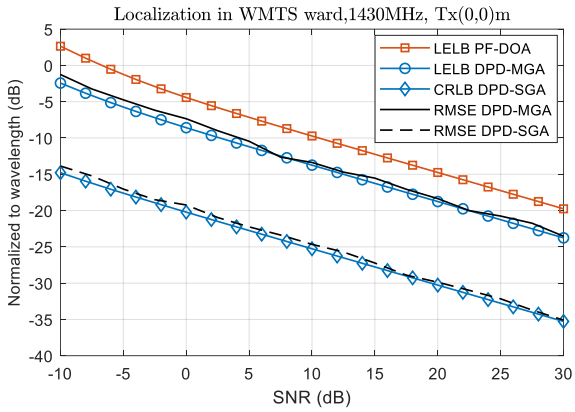

Fig. 7: The performance comparison for DPD and PF-DOA in an indoor application with the array depicted in Fig. 6 using both MGA and SGA structures

6. Conclusion

In this paper, we derived the formulations of CRLB and LELB for DPD and PF-DOA techniques of localization of co-channel signals for outdoor and indoor applications. By comparing the LELBs for outdoor applications, we showed that DPD can achieve localization RMSE of about 3dB lower than the PF-DOA method, which is a noticeable improvement because this means that the effective depth of the operational field has been enlarged by about 70%.

For indoor applications, we first showed that DPD with MGA structure outperforms the PD-DOA by about 5 dB. Also, we pointed out the opportunity of using an SGA

structure instead of the commonly used MGA structure and proved the superiority of using SGA over MGA by about 13dB in localization accuracy, which is a significant enhancement in accuracy for indoor localization applications.

CRediT Authorship Contribution Statement

Ali Eshkevari: Conceptualization, Investigation, Writing - original draft. **Seyed Mohammad Sajad Sadough:** Formal analysis, Supervision, Writing - review & editing.

Declaration of Competing Interest

The authors declare that they have no known competing financial interests or personal relationships that could have appeared to influence the work reported in this paper. The ethical issues; including plagiarism, informed consent, misconduct, data fabrication and/or falsification, double publication and/or submission, redundancy has been completely observed by the authors.

References

[1] H. Lai and K. Bell, "Cramer-rao lower bound for DOA Estimation using vector and higher-order sensor arrays," in *Conference Record of the Forty-First Asilomar Conference on Signals*, Systems and Computers, Asilomar, 2007, pp. 1262-1266.

[2] Z.-M. Liu, "Conditional Cramér–rao lower bounds for DOA estimation and array calibration," *IEEE Signal Processing Letters*, vol. 21, no. 3, pp. 361-364, 2014.

[3] L. Kumar and R. M. Hegde, "Stochastic cramér-rao bound analysis for DOA estimation in spherical sarmonics somain," *IEEE Signal Processing Letters*, vol. 22, no. 8, pp. 1030-1034, 2015.

[4] M. Trinh-Hoang, M. Viberg, and M. Pesavento, "Cramér-rao bound for DOA estimators under the partial relaxation framework: derivation and comparison," *IEEE Transactions on Signal Processing*, vol. 68, pp. 3194-3208, 2020.

[5] J. Li, I.-T. Lu and J. Lu, "Cramer-rao lower bound analysis of data fusion for fingerprinting localization in non-line-of-sight environments," *IEEE Access*, vol. 9, pp. 18607-18624, 2021.

[6] Y. Liang, W. Cui, and H. Wu, "Cramér-rao bound for DOA estimation exploiting multiple frequency pairs," *IEEE Signal Processing Letters*, vol. 28, pp. 1210-1214, 2021.

[7] A. J. Weiss, "Direct position determination of narrowband radio frequency transmitters," *IEEE Signal Processing Letters*, vol. 11, no. 5, pp. 513-516, May 2004.

[8] L. Tzafri and A. J. Weiss, "High-resolution direct position determination using MVDR," *IEEE Transactions on Wireless Communications*," vol. 15, no. 9, pp. 6449-6461, Sept 2016.

[9] A. Amar and A. J. Weiss, "Direct position determination of multiple radio signals," *EURASIP Journal of Applied Signal Processing*, pp. 37-49, Jan. 2005.

[10] T. Tirer and A. J. Weiss, "High resolution direct position determination of radio frequency sources," *IEEE Signal Processing Letters*, vol. 23, no. 2, pp. 192-196, Feb. 2016.

[11] T. Tirer and A. J. Weiss, "Performance analysis of a high-resolution direct position determination method," *IEEE Transactions on Signal Processing*, vol. 65, no. 3, pp. 544-554, Feb. 2017.

[12] A. J. Weiss, "Direct geolocation of wideband emitters based on delay," I*EEE Transactions on Signal Processing*, vol. 59, no. 6, pp. 2513–2521, 2011.

[13] O. Bar-Shalom, "Efficient direct position determination of orthogonal frequency division multiplexing signals," *IET Radar, Sonar and Navigation*, vol. 3, no. 2, pp. 101–111, 2009.

[14] L. Huang and L. Yilong, "Performance analysis of direct position determination for emitter source positioning," *American Journal of Signal Processing*, vol. 2, no. 3, pp. 41-45, 2012.

[15] F. Chen and T. Zhou, "Direct position determination and effective extraction of multiple transmitters," *IET Journal of Engineering* , vol. 5, no. 21, pp. 7787--7791, 2019.

[16] A. Eshkevari and S. M. S. Sadough, "Enhanced direct position determination using dynamic sensor array response," *IET Electronics Letters*, vol. 56, no. 7, pp. 354-357, 2020.

[17] J. Du, H. Yu and G. Liu, "Unified subspace fitting framework and its performance analysis for direct position determination in the presence of multipath propagation," *IEEE Access*, vol. 7, pp. 6889-6914, 2019.

[18] F. Ma, Z.-M. Liu, and F. Guo, "Direct position determination in asynchronous sensor networks," *IEEE Transactions on Vehicular Technology*, vol. 68, no. 9, pp. 8790-8803, sep, 2019.

[19] Y. Ye, U. Khan, and K. Pahlavan, "On the accuracy of RF positioning in multi-capsule endoscopy," in *IEEE 22nd International Symposium on Personal, Indoor and Mobile Radio Communications*, Toronto, 2011, pp. 2173-2177.

[20] S. T. Goh, S. A. Zekavat, and K. Pahlavan, "DOA-based endoscopy capsule localization and orientation estimation via unscented kalman filter," *IEEE Sensors Journal*, vol. 14, no. 11, pp. 3819-3829, 2014.

[21] H. Wang, Y. Zhang, and G. Wang, "Positioning algorithm for wireless capsule endoscopy based on RSS," in *IEEE International Conference on Ubiquitous Wireless Broadband (ICUWB)*, Nanjing, 2016, pp. 1-3.

[22] F. Bianchi, A. Masaracchia, and E. Shojaei, "Localization strategies for robotic endoscopic capsules: a review," *Taylor & Francis - Expert Review of Medical Devices*, vol. 16, pp. 381-403, 2019.

[23] H. L. Van Trees, Optimum array processing, new york: John Wiley & Sons, Inc., 2002.

[24] O. Bar-Shalom and A. J. Weiss, "Direct positioning of stationary targets using MIMO radar," *Elsevier Journal of Signal Processing*,vol. 91, no. 10, pp. 2345-2358, 2011.

[25] F.C.C., "FCC Rules: Regulations for Title 47 C.F.R.," F.C.C., 2019.

BIOGRAPHY

Ali Eshkevari was born in Tehran, Iran, in 1968. He received the B.Sc. degree in electrical engineering (electronics) from the Khajeh Nasir Toosi University of Technology, Tehran, in 1991, and the M.Sc. degree in electrical engineering (telecommunication systems) from the Amirkabir University of Technology, Tehran, in 1997. He is currently pursuing the Ph.D. degree with the Electrical Engineering Department, Shahid Beheshti University, Tehran. His Ph.D. thesis is on direct position determination of radio signals.

Seyed Mohammad Sajad Sadough was born in 1979. He received the B.Sc. degree in electrical engineering (electronic) from Shahid Beheshti University, Tehran, Iran, in 2002, and the M.Sc. and Ph.D. degrees in electrical engineering (telecommunication) from Paris-Saclay University, Orsay, France, in 2004 and 2008, respectively. During his Ph.D. (2004–2007), he was with the Institut Polytechnique de Paris (ENSTA), Paris, France, and Centrale Supélec—CNRS/Laboratory of Signals and Systems (LSS), Gif-sur-Yvette, France. He has been a Lecturer with the Electronics and Computer Engineering Department, ENSTA, where his research activities were focused on improved reception schemes for ultra-wideband communication systems. From December 2007 to September 2008, he was a Postdoctoral Researcher at Centrale Supélec—CNRS/LSS, where he was involved in research projects with Alcatel-Lucent on satellite mobile communication systems. In October 2008, he joined the Faculty of Electrical Engineering, Shahid Beheshti University, where he is currently an Associate Professor with the Telecommunication Department. His current research interests include optical wireless communications, signal processing for wireless communications, with particular emphasis on multicarrier and MIMO systems, joint channel estimation and decoding, iterative reception schemes, and receiver design under partial channel state.